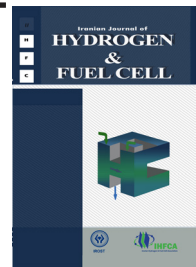


Iranian Journal of Hydrogen & Fuel Cell

IJHFC

Journal homepage://ijhfc.irost.ir



Investigation and optimization of a PEM fuel cell's electrical and mechanical behavior

Mostafa Habibnia¹, Mohsen Shakeri², Salman Nourouzi³, Peyman Ghasemi Tamami^{4,*}

¹Mechanical Engineering Department, Babol University of Technology, Babol, Iran

²Mechanical Engineering Department, Babol University of Technology, Babol, Iran

³Mechanical Engineering Department, Babol University of Technology, Babol, Iran

⁴Mechanical Engineering Department, Islamic Azad University, Sari, Iran

Article Information

Article History:

Received:

20 March 2016

Received in revised form:

28 May 2016

Accepted:

31 May 2016

Keywords

Proton exchange membrane fuel cell

Clamping pressure

Electrical resistance

Uniform pressure

Abstract

The effect of clamping pressure on electrical resistance between the Gas diffusion layer (GDL) and bipolar plate is a very important parameter in Proton exchange membrane (PEM) fuel cells. There have been several studies done in the last few years to investigate this matter, but there have not been any experimental investigations of the clamping pressure effect on PEM electrical resistance. In this paper, experimental tests were performed with various clamping pressures in order to find the relationship between clamping pressure and electrical resistance. These same situations were also simulated in Abaqus software and their results were then compared to each other. Models of different situations of clamping pressure and thicknesses of end plate for uniform pressure distribution on the gas diffusion layer have been obtained and these models were investigated for electrical analysis. These models have been imported for electrical and mechanical analysis with putting electrical loads and boundary conditions. Finally, results of the investigation showed that a PEM fuel cell with more clamping pressure and end plate thickness has less electrical resistance. Stress and electrical resistance have a reversed relationship to each other. In other words, increasing the clamping pressure will reduce the electrical resistance between the gas diffusion layer and bipolar plate and vice versa.

1. Introduction

Fuel cells are devices that directly convert the chemical energy of a fuel into electrical energy. Unlike internal combustion engines there is no burning of the fuel and therefore no generation of airborne pollutants. Due to its high efficiency and cleanliness as a power source,

fuel cells have attracted interest from government agencies, academia, scientific laboratories and industry [1-8]. In a typical fuel cell, hydrogen and oxygen react electrochemically at separate electrodes producing electricity, heat, and water. Power specifications can be met by connecting a specific number of cells in series to generate the necessary voltage and by sizing

*Corresponding Author's E-mail address: engghasemi696@gmail.com

the active area of the cells to obtain the amperage needed.

It provides the electrical connectivity from cell to cell, and it separates the reactive gases. On the anode side of the plate, hydrogen gas is consumed to produce electrons and protons, as in Eq. (1). The electrons are collected by the anode and the protons enter the electrolyte. On the other side of the plate, on the cathode side, oxygen gas combines with electrons from the cathode and protons from the electrolyte to produce water, as in Eq. (2):



The proton exchange membrane fuel cell (PEMFC) has attracted much attention as a promising power source with wide application owing to its high power efficiency, high energy density, quick cold-start capability and low level of pollution [9-12]. It is a possible substitute for combustion engines in automobiles and heat generators in houses. For PEMFCs to meet the requirements of practical applications, their performance and lifetime need to be optimized. As the voltage and total power generated by a single cell PEMFC is rather limited, PEMFC products for practical applications comprise numerous planar single cells in series that form large stack structures with a cyclic cell characteristic. Typically, two end plates, between which the unit cells are inserted, are located on the outside of the stack to provide proper internal compression, and the entire fuel cell structure is fastened with a set of bolts or by another fastening mechanism. End plates need to be well designed to have sufficient mechanical strength and stiffness while consisting of a minimum amount of materials. A good design of the PEMFC stack requires that the contact pressure in each cell is not only approximately equal but also has as uniform a distribution as possible [13]. In general, there may be high contact electrical resistance at the interface between the gas diffusion layer (GDL) and the bipolar plate (BPP), as shown in Fig. 1, if the contact pressure is

unreasonably small [14-16]. However, the permeability of the GDL will be too low to provide high reaction efficiency if the contact pressure is excessively large [17]. Contact resistance is determined by the material properties, surface topology, and assembly pressure and operation conditions. During assembly, an optimal assembly pressure is needed to balance the contact resistance and flow resistance in GDL [18]. A high assembly pressure can reduce the contact resistance, but the GDL will be over compressed with high stress, which results in increased flow resistance. Thus, understanding the contact resistance mechanisms between BPP and GDL is important in optimizing clamping pressure as well as improving the fuel cell performance.

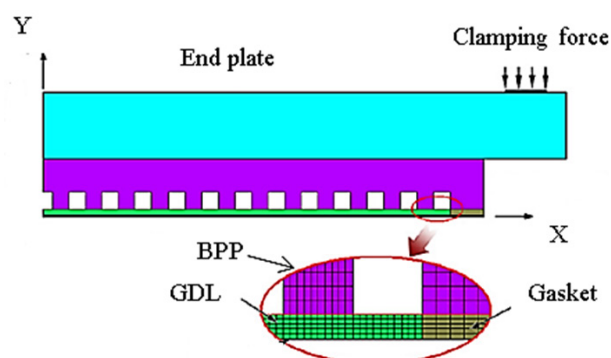


Fig. 1. Contact between BPP and GDL.

Experimental research and FEM models on the contact resistance have been reported in the following literature. Wang [19] studied the contact resistances between carbon paper and different stainless steels and found that 349TM is the best candidate for bipolar plate material in PEM fuel cells for lowering interfacial electrical resistance. Mishra [20] conducted experiments to show the effects of different GDL materials and contact pressure on the electrical contact resistance. Itonen [21] developed a novel PEM fuel cell assembly to measure the clamping pressure and contact resistances simultaneously. Lee [22] conducted experiments to measure the PEM fuel cell performance on different types of GDL and found that each type of GDL has its own optimal clamping pressure. Chang [23] measured contact resistance between BPP and GDL using a specially designed test rig

under various clamping pressure levels. The results also showed that there should be a trade-off of the clamping pressure to optimize the contact resistance and mass transfer. Ge [24] studied the effects of GDL compression on fuel cell performance using a unique fuel cell test fixture. Lee [25] proposed a FEM model and analyzed the MEA pressure distribution under given assembly pressure in a single cell. Zhou [14] developed a FEM model to analyze the ohmic contact resistance between the BPP and the GDL, the GDL deformation, and the GDL porosity distribution. However, the electrical contact resistance is a parameter of the electrical field while the contact pressure has to be obtained by a mechanical analysis. Moreover, the electrical contact resistance is dependent on the contact pressure. Thus, prediction of the electrical contact resistance is a coupled mechanical–electrical problem. Attempts have been made in the past to decouple the solution. For example, Zhou [14] and Zhang [26] developed mechanical FEM models to first obtain the contact pressure and contact area for each contact element, and then calculate the contact resistance based on a contact resistance pressure constitutive relation. In their FEM models, the contact resistance is calculated based on the assumption that the contact surface is equipotential and the electric circuit of the contact surface is in a parallel connection. More recent research on electrical and mechanical analysis of PEMFC include the discussion and prediction of analytical models of fuel cells properties. A lack of experimental tests and software modeling in this context for more accurate results is very sensible. FoTo this aim, in this research experimental and software modeling have been done to study PEMFC electrical and mechanical properties with more accuracy and the relationships between PEMFC's electrical and mechanical parameters have been studied.

2. Experimental

Experimental tests were conducted to investigate the electrical resistance of PEM fuel cells. A method for

quick evaluation of electrical interfacial resistance between each candidate material and other materials was developed. The setup's components were cut into plates of 3 mm thickness and 5×5 area for contact resistance measurements as shown in Fig. 2.

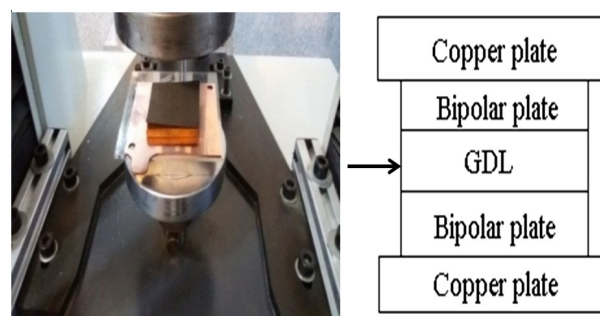


Fig. 2. Assembled setup for testing.

Contact resistance measurements are conducted with a setup as shown in Fig. 2. For calculating contact resistance between setup components, a hydraulic press is used to provide a series of prescribed clamping pressures between 0.1-2 MPa as shown in Fig. 3.

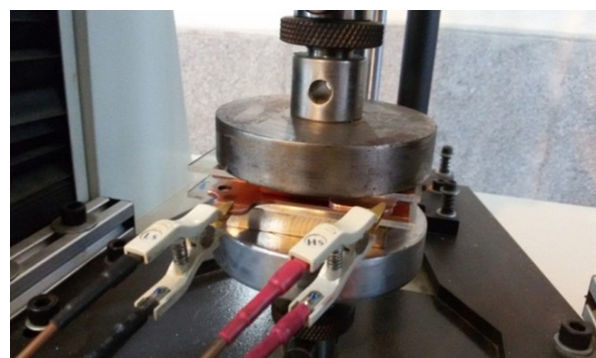


Fig. 3. Setup under hydraulic press.

In the experimental tests, a series of clamping pressures were applied and the corresponding contact resistances were measured. As seen in Fig. 4, a DC current is applied by the source meter and the potential drop is measured to calculate the total resistance (R_{Total}) to the setup assembly. This setup accuracy is 0.01 mΩ and all values have been measured with this accuracy. Fig. 5a shows the setup for determining interfacial resistance between components. This setup was constructed from several components, and the relationship between them is shown in Eq. (3). All



Fig. 4. Electrical resistance measuring device.

parameters in Eq. (3), except $R_{BPP/GDL}$ and $R_{BPP/Cu}$, are available in handbooks. Two other setups has been made for calculating other parameters as shown in Figs. 5a, b. Setup 2 was built using a stack of GDL and thin Copper plate as shown in Fig. 5b. This stack was inserted between two Copper plate current collectors. Plexiglas plates were used for insulation. The surfaces of the polished Copper plate and the GDL are cleaned with isopropanol and dried to remove any particle debris. The measured resistance from Setup 2 includes the bulk resistances of three Copper plates, the bulk resistance of GDL, and the contact resistances between Copper plates and GDL as shown in Eq. (4). Setup 3 uses a similar stack with only one BPP between two Copper plates, as shown in Fig. 5c, in order to extract the contact resistance between BPP and Cu as shown in Eq. (5).

$$2R_{Cu} + 2R_{BPP} + R_{GDL} + 2R_{BPP/Cu} + 2R_{BPP/GDL} = \frac{VIA}{I} \quad (3)$$

$$3R_{Cu} + R_{GDL} + 2R_{Cu/GDL} = \frac{V2A2}{I2} \quad (4)$$

$$2R_{Cu} + R_{BPP} + 2R_{BPP/Cu} = \frac{V3A3}{I3} \quad (5)$$

Table 1 shows some obtained results for R_{total} in the different setups of Fig. 5 after experimental tests.

By using Table 1 and Eqs. (3-5), electrical resistance has been investigated with an accuracy of 0.01 mΩ between each component, and their relationship with clamping pressure is shown in Fig. 6. BPP was made of Graphite plates and has its properties.

Some parameters that are used for software modeling have been extracted from experimental test results and the Wang test setup components [19] have been used for the experimental testing and modeled in Abaqus® software as shown in Fig. 7. Those situations were then simulated in software to compare the experimental and simulation results. For this matter setup components have been modeled in the same size and thickness and rows as shown in Fig. 8, and material properties have been defined for the software as shown in Table 2. For the electrical-mechanical analysis in the in Interaction Module of the software, Gap electrical conductance between the setup components should be defined as shown in Fig. 9. These values have been imported into the software from primary experimental tests and calculation as shown in Eqs. (6-9).

$$R = \frac{V}{I} \quad (6)$$

The resistance R of an object is defined as the ratio of voltage of V across to the object through the current of I as shown in Eq. (6).

$$R = \rho \times \frac{L}{A} \quad (7)$$

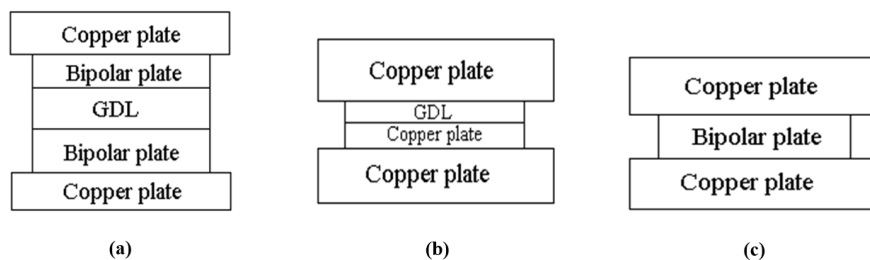


Fig. 5. Schematic of the contact resistance measurement setups.

Table 1. Electrical Resistance Results of Tests

Test number	Hydraulic pressure (MPa)	Rtotal of setup 1 (mΩ)	Rtotal of setup 2 (mΩ)	Rtotal of setup 3 (mΩ)
1	0.1	32.00	6.75	19.80
2	0.2	16.81	3.73	10.63
3	0.3	11.56	2.76	7.34
4	0.4	9.15	2.19	5.56
5	0.6	6.53	1.67	3.93
6	0.8	5.07	1.29	3.18
7	1	4.15	1.09	2.65
8	1.2	3.63	0.96	2.29
9	1.6	2.89	0.78	1.85
10	2	2.46	0.63	1.56

Where L is the length of the piece of material, A is cross-sectional area of the specimen, ρ is the electrical resistivity, and R is the electrical resistance as shown in Eq. (7).

$$\sigma = \frac{1}{\rho} \tag{8}$$

Using Eq. (7), Conductivity σ is defined as the inverse of resistivity as shown in Eq. (8).

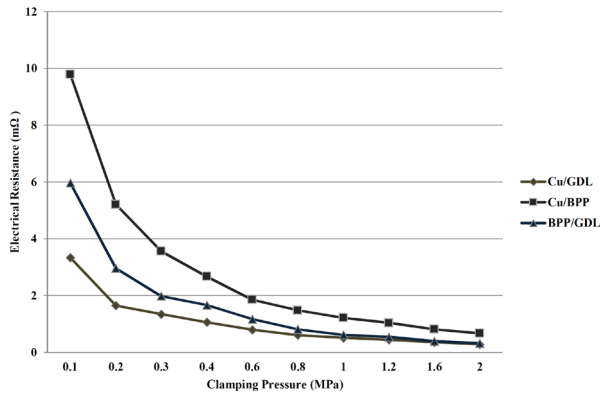


Fig. 6. Experimental results of the components contact electrical resistance dependent on clamping pressure.

$$\rho = \frac{E}{J} \tag{9}$$

Where E is the magnitude of the electric field and J is the magnitude of the current density, ρ can be defined as shown in Eq. (9).

Using Eqs (6-8) and dimensions (50*50 mm) for the components for the parameter of A and electrical resistance as shown in Fig. 6 of parameter R and the unit value for the L parameter, ρ is calculated and then by inserting it in Eq. (8) the gap electrical conductance is calculated as shown in Fig. 9. Eq. (9) is about calculating the magnitude of electric field used for software modeling.

Software modeling of the Wang setup in Abaqus® software needs some special care as to be explained below. This model will be run in software with a Coupled Electrical-Thermal-Structural step. In addition to the mechanical definitions, some electrical parameters should be defined for the model in the property module as shown in Table 2.

Because of the electrical-mechanical analysis in this

Table 2. Properties of the Constructed Setup Components

Component	Material	Density (Kg/m³)	Young's Modulus (GPa) [27]	Poisson's Ratio	Electrical Conductivity (S/m)
Electrode	Copper	8900	110	0.37	59600000
BPP	Graphite	2000	0.12	0.25	100000
GDL	Porous Carbon	440	0.0061	0.3	1250

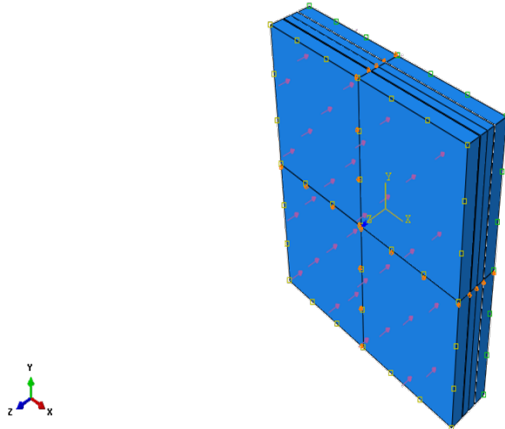


Fig. 7. Simulated model of setup with applied loads.

Copper plate
GDL
Bipolar plate
GDL
Copper plate

Fig. 8. Setup model for validating experimental and software simulation.

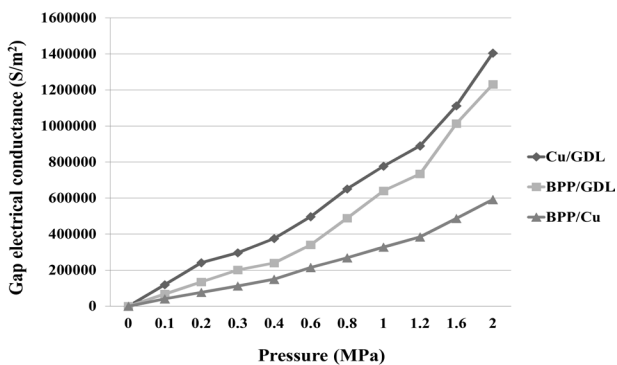


Fig. 9. Gap electrical conductance is dependent on the pressure between components.

model, electrical behavior should be defined between components as shown in Fig. 9. Electrical loads and boundary conditions should be defined for the setup, and the element type for this analysis is Quasi-three-dimensional eight-noded quadrilateral isoparametric elements (Q3D8). After modeling all parameters with the software and analyzing the model, all results of

software and experimental tests have been compared as shown in Fig. 10.

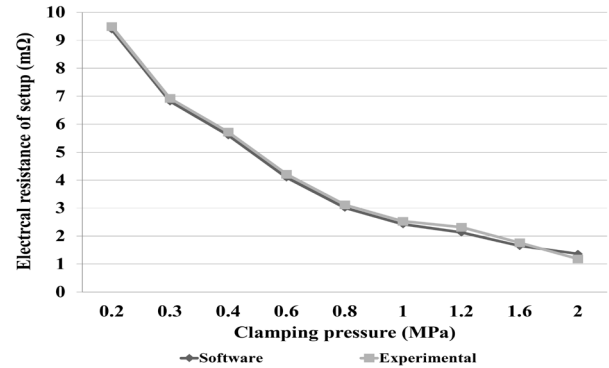


Fig. 10. Experimental and software results of the setup's electrical resistance.

3. Electrical-Mechanical analysis of PEM fuel cells

All components of the PEM fuel cell have been modeled in software for the Electrical-Mechanical analysis. A single cell of a PEM fuel cell has been created from several components including an end plate, copper plate, bipolar plate, gasket and gas diffusion layer as shown in Fig. 11. Fuel cell components have been modeled in software at the same size as the real one. End plates are 109×116 mm and Copper plates and BPPs are 80×87 mm and GDL is 50×50 mm. The components properties defined as shown in Table 3 are the results of experimental tests while others have been obtained from recent research.

As shown in Table 3, the Gasket has hyper elastic behavior and uniaxial test data are used for definition of hyper elastic material for the software as shown in Fig. 12.

After definition of the property and step module, the assembly module was done as shown in Fig. 13. The assembled model was loaded with the clamping pressures, electrical surface currents, and electrical-mechanical boundary conditions and was meshed with a Quasi-three-dimensional eight-noded quadrilateral isoparametric (Q3D8) element type.

Some parameters such as clamping pressure, number of bolts, end plate thickness and bipolar groove have

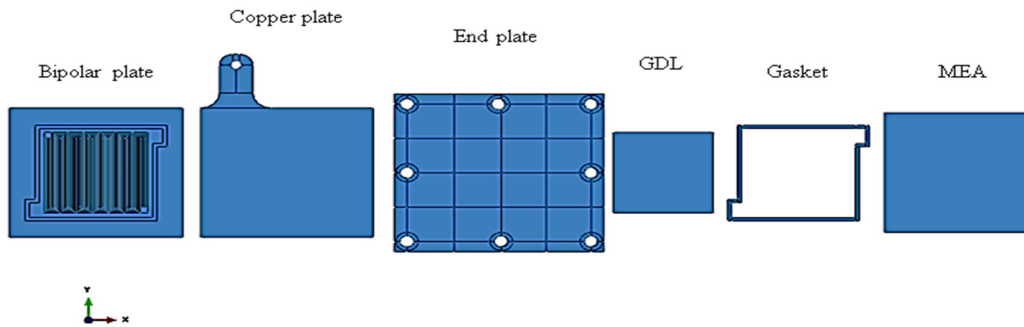


Fig. 11. Components of one stack PEM fuel cell.

Table 3. Properties of PEM Fuel Cell Components [27]

Part	Material	Mechanical Behavior	Young's Modulus (GPa)	Poisson's Ratio	Density (Kg/m ³)	Electrical Conductivity (S/m)
End Plate	Steel	Elastic	210	0.3	7850	59000000
Copper Plate	Copper	Elastic	110	0.37	8900	59600000
Gasket	Polymer	Hyper elastic	-	-	2330	1000
BPP	Graphite	Elastic	0.12	0.25	2000	100000
GDL	Porous Carbon	Plastic	0.0061	0.3	440	1250

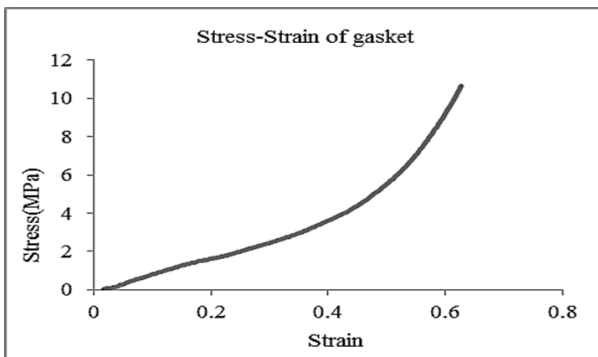


Fig. 12. Gasket stress-strain diagram.

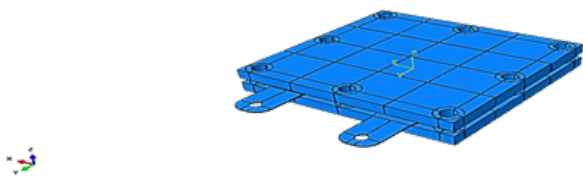


Fig. 13. Assembly model of PEM fuel cell.

been studied to analyze the PEM mechanical behavior and better configure the cell to achieve more uniform

stress distribution on GDL, and after calculating of standard deviation of stress of 10 Bar on GDL as shown in Eqs. (10-11), the optimized model was selected. Parameters of the PEM fuel cell model which has good uniform stress distribution on GDL have been investigated as shown in Fig. 14.

Where X is a random variable with a mean value μ as in Eq. (10), and a standard deviation of σ will be as shown in Eq. (11).

$$\mu = (X_1 + X_2 + X_3 + \dots + X_n) \tag{10}$$

$$\sigma = \sqrt{\frac{\sum_1^N (X_i - X_n)^2}{N}} \tag{11}$$

Fig. 15 shows some path states of stress created by BPP on GDL by clamping pressure for one of the PEM fuel cells. This figure shows that the stress on GDL is symmetric and the center of the GDL has the lowest amount. As shown in Fig. 16, BPP has ten grooves and creates ten areas of stress on the GDL. Because of fuel cell symmetry, the upper half five

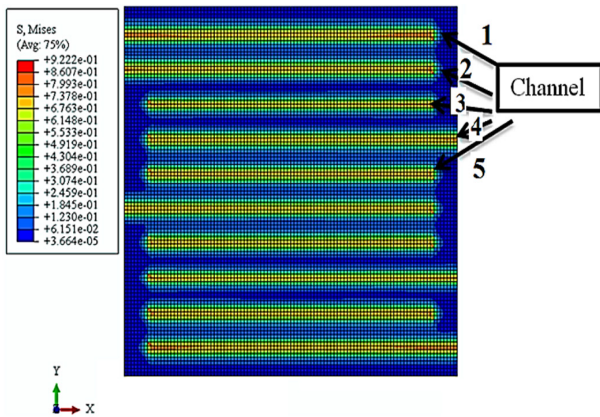


Fig. 14. Stress contour on GDL on the best PEM configuration.

paths and lower half five paths have equal stress, so for this work the five paths of upper half area of the GDL have been investigated.

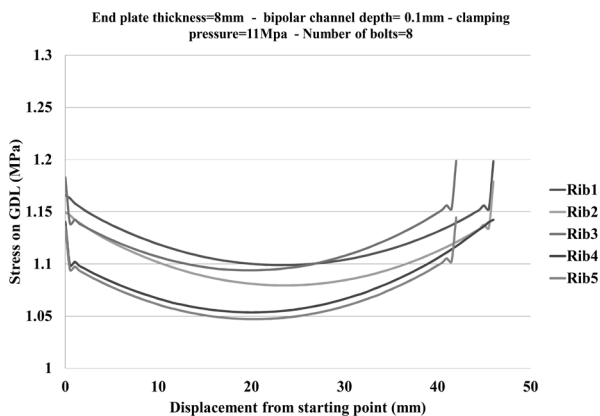


Fig. 15. Stress on GDL in five paths of the upper half of the GDL.

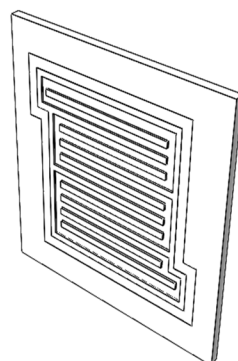


Fig. 16 Schematic of bipolar plate and its channels.

After mechanical analysis and selecting the best configuration for uniform pressure distribution, some models have been imported for electrical analysis and

investigation of the relationship between clamping pressure and electrical current per unit area and electrical resistance on this fuel cell. Contour of the electrical current per unit area passing from GDL has been showed in Fig. 17.

To investigate the relationship between electrical resistance and clamping pressure and end plate thickness of one stack PEM fuel cell, nine different conditions for the PEM fuel cell have been modeled in the software and their results have been shown in Fig. 18. In this step a whole model of the PEM fuel cell has been analyzed in software, and in the last step the electrical resistance of the PEM fuel cell has been calculated from software outputs in different situations as shown in Fig. 18.

4. Conclusion

Attention to the results showed that increasing clamping pressure in fuel cells and setups can improve electrical efficiency and decrease electrical resistance and energy losses. Clamping pressure should be increased to a level that decreases electrical resistance as much as possible, but too much clamping pressure damages the fuel cell structure. Results show that as end plates thickness increases, electrical resistance is reduced and this was investigated at thicknesses of 8, 10 and 12 mm. Using these analyses, industry can build fuel cells with higher efficiency and less power losses which are related to the contact resistance between GDL and BPP. In industrial applications uniform stress distribution on GDL and minimum standard deviation and less power losses are important parameters for fuel cells selections and with this research we can select an optimized model of a PEM fuel cell.

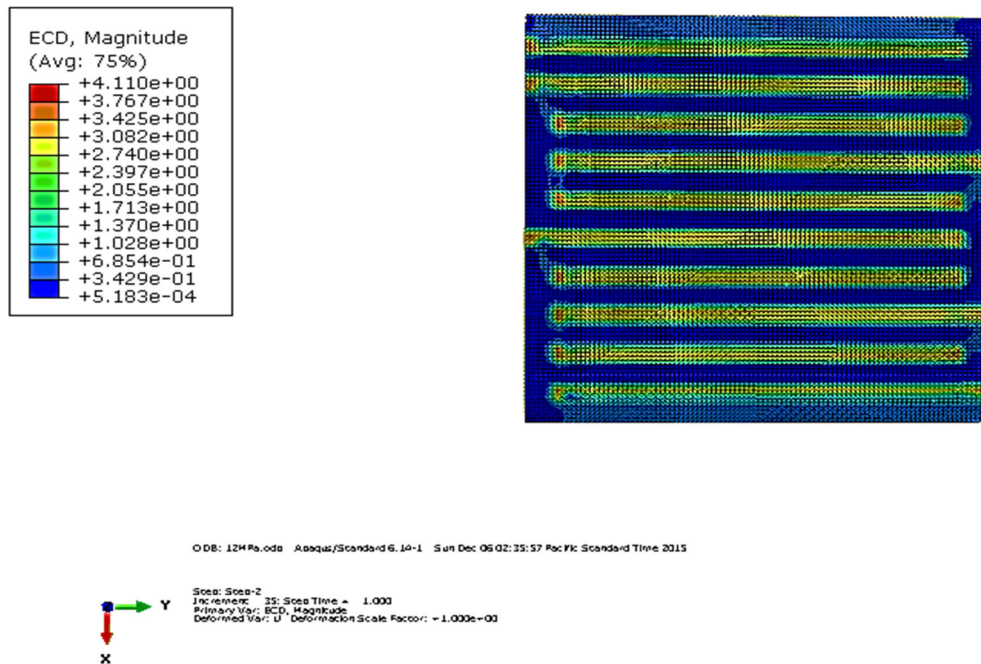


Fig. 17 Electrical current per unit area contour in GDL.

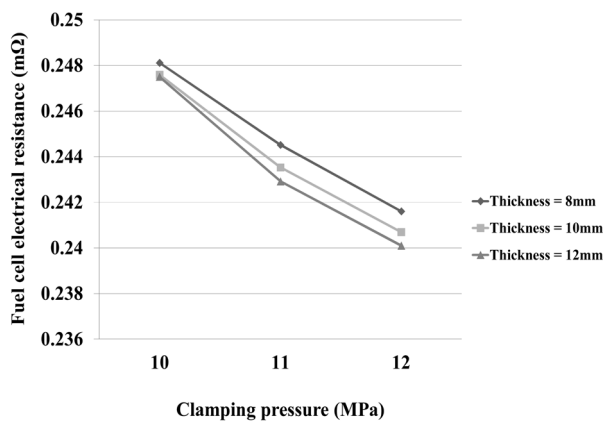


Fig. 18. The relationship between electrical resistance of a PEM fuel cell and clamping pressure with end plates with different thicknesses.

5. References

- [1] B.C.H. Steele, A. Heinzel, Nature (London) 414.6861 (2001): 345-352.
- [2] S.J.C. Cleghorn, X. Ren, T. Espringer, M.S. Wilson, C. Zawodzinski, T.A. Zawodzinski, S. Gottesfeld, Int. J. Hydrogen Energy 22.12 (1997): 1137-1144.
- [3] D. Chu, R. Jiang, J. Power Sources 80.1 (1999): 226-234.
- [4] J. Itonen, F. Jaouen, G. Lindbergh, G. Sundholm, Electrochim. Acta 46.19 (2001): 2899-2911.
- [5] C.E. Borroni-Bird, J. Power Sources 61.1 (1996): 33-48.
- [6] K.B. Prater, J. Power Sources 61.1 (1996) 105-109.
- [7] W. Smith, J. Power Sources 86.1 (2000) 74-83.
- [8] O.J. Murphy, A. Cisar, E. Clarke, Electrochim. Acta 43.24 (1998) 3829-3840.
- [9] R.V. Helmolt, U. Eberle, J. Power Sources 165 (2007) 833-843.
- [10] A. Kundu, J.H. Jang, J.H. Gil, C.R. Jung, H.R. Lee, S.H. Kim, B. Ku, Y.S. Oh, J. Power Sources 170 (2007) 67-78.
- [11] A.S. Patil, T.G. Dubois, N. Sifer, E. Bostic, K. Gardner, M. Quah, C. Bolton, J. Power Sources 136 (2004) 220-225.

- [12] M. Uzunoglu, O.C. Onar, M.S. Alam, J. Power Sources 168 (2007) 240–250.
- [13] S. Karvonen, T. Hottinen, J. Itonen, H. Uusalo, ASME J. Fuel Cell Sci. Technol. 5 (2008) 1–9.
- [14] P. Zhou, C.W.Wu, G.J. Ma, J. Power Sources 159 (2006) 1115–1122.
- [15] P. Zhou, C.W. Wu, G.J. Ma, J. Power Sources 163 (2007) 874–881.
- [16] P. Zhou, C.W.Wu, J. Power Sources 170 (2007) 93–100.
- [17] L. Cinderlla, A.M. Kannan, J.F. Lin, K. Saminathan, Y. Ho, C.W. Lin, J. Wertz, J. Power Sources 194 (2009) 146–160.
- [18] S.J. Lee, C.D. Hsu, C.H. Huang, J. Power Sources 145 (2005) 53–361.
- [19] H.L.Wang, M.A. Sweikart, J.A. Turner, J. Power Sources 115 (2003) 243–251.
- [20] V. Mishra, F. Yang, R. Pitchumani, ASME J. Fuel Cell Sci. Technol. 1 (2004) 2–9.
- [21] J. Itonen, F. Jaouen, G. Lindbergh, G. Sundholm, Electrochim. Acta 46 (2001) 2899–2911.
- [22] W.-K. Lee, C.-H. Ho, J.W. Van Zee, M. Murthy, J. Power Sources 84 (1999) 45–51.
- [23] W.R. Chang, J.J. Hwang, F.B. Weng, S.H. Chan, J. Power Sources 166 (2007) 149–154.
- [24] J. Ge, A. Higier, H. Liu, J. Power Sources 159 (2006) 922–927.
- [25] S.J. Lee, C.D. Hsu, C.H. Huang, J. Power Sources 145 (2005) 353–361.
- [26] L. Zhang, Y. Liu, H. Song, S.Wang, Y.Y. Zhou, S.J. Hu, J. Power Sources 162 (2006) 1165–1171.
- [27] Lai, Xinmin, Linfa Peng, and Jun Ni. "A mechanical–electrical finite element method model for predicting contact resistance between bipolar plate and gas diffusion layer in PEM fuel cells." Journal of Power Sources 182.1 (2008): 153-159.